Localization of Primary Prostate Cancer with Dual-Phase ^{18}F-Fluorocholine PET

Sandi A. Kwee, MD[1,2]; Hai Wei, PhD[3]; Isabell Sesterhenn, MD[4]; David Yun, PhD[5]; and Marc N. Coel, MD[1]

[1]Hamamatsu/Queen's PET Imaging Center LLC, Honolulu, Hawaii; [2]Department of Medicine, John A. Burns School of Medicine, University of Hawaii at Manoa, Honolulu, Hawaii; [3]i.Solutions, Inc., Honolulu, Hawaii; [4]Armed Forces Institute of Pathology, Washington, DC; and [5]Laboratory of Intelligent and Parallel Systems, College of Engineering, University of Hawaii at Manoa, Honolulu, Hawaii

This study compared ^{18}F-fluorocholine uptake in malignant and benign areas of the prostate at 2 time points to determine the suitability of delayed or dual-phase ^{18}F-fluorocholine PET for localizing malignancy in the prostate gland. **Methods:** Twenty-six men (15 newly diagnosed with prostate cancer, 2 with recurrent prostate cancer, 6 with no evidence of prostate cancer recurrence after treatment, and 3 with no history of prostate cancer) underwent dual-phase PET consisting of initial whole-body PET starting 7 min after injection of 3.3–4 MBq/kg of ^{18}F-fluorocholine followed by 1-h delayed PET of the pelvis. Tracer uptake in the prostate on the initial and delayed images was measured on a sextant basis. Prostate biopsy or whole-prostate histologic examination after radical prostatectomy was used to classify a prostate sextant as a dominant malignant region or probable benign region. For each sextant, a retention index based on the measured maximum standardized uptake value (SUVmax) was calculated on the initial and delayed images. In 15 prostates with both benign and malignant sextants on histologic examination, a malignant-to-benign ratio of SUVmax was also calculated for each time point. **Results:** A dominant malignant region was found in 17 subjects, and a probable benign region was found in 24 subjects. The mean SUVmax for dominant malignant regions increased significantly between initial and delayed scans, from 7.6 to 8.6 (mean retention index, +14%; 95% confidence interval, 6%–22%; $P = 0.002$). The mean SUVmax for probable benign regions decreased significantly between initial and delayed scans, from 4.8 to 3.9 (mean retention index, −17%; 95% confidence interval, −10% to −23%, $P < 0.001$). The mean malignant-to-benign ratio increased significantly, from 1.4 on the initial scan to 1.8 on the delayed scan ($P = 0.003$). The areas under the receiver operating characteristic curves for distinguishing dominant malignant regions from probable benign regions based on initial SUVmax, delayed SUVmax, and retention index were 0.81, 0.92, and 0.93, respectively. **Conclusion:** On dual-phase PET of the prostate, areas of malignancy consistently demonstrated stable or increasing ^{18}F-fluorocholine uptake, whereas most areas containing benign tissue demonstrated decreasing uptake. Delayed or dual-phase imaging after injection of ^{18}F-fluorocholine may improve the performance of ^{18}F-fluorocholine PET for localizing malignant areas of the prostate.

Received Jul. 28, 2005; revision accepted Nov. 7, 2005.

For correspondence or reprints contact: Sandi A. Kwee, MD, Nuclear Medicine Department, Queen's Medical Center, 1301 Punchbowl St., Honolulu, HI 96813.

E-mail: skwee@queens.org

Key Words: PET; prostatic neoplasms; fluorocholine

J Nucl Med 2006; 47:262–269

Prostate cancer is the second leading cause of cancer death in American men older than 50 y. Potentially curative treatment options for organ-confined prostate cancer include radical prostatectomy and radiation therapy. However, these definitive treatments are not without significant clinical side effects. To optimally treat subjects at this early stage, knowledge of the location and extent of cancer within the prostate may prove useful. For example, the locations of malignant sites within the prostate could be incorporated into a radiation therapy strategy to augment radiation dose to malignant areas while maintaining a safer dose to sensitive critical structures (*1,2*). Because the success rate and morbidity of prostate radiation therapy is directly related to radiation dose (*3*), such an individualized approach could conceivably improve both the safety and the efficacy of this method of treatment.

Unfortunately, despite advances in the technology of ultrasound, CT, and MRI, it remains difficult to locate malignant sites within the prostate (*4*). This difficulty in localization extends to sampling of the prostate at biopsy, which may detect only 50% of the malignant areas found on histologic examination of the whole prostate (*5*). A false-negative cancer detection rate exceeding 20% for transrectal ultrasound-guided prostate sextant (i.e., 6 regions) biopsy often makes it necessary to consider repeating biopsies in subjects with persistently elevated serum levels of prostate-specific antigen (PSA) and negative initial biopsy results (*6,7*). Unfortunately, simply increasing the number of biopsy samples does not necessarily result in higher detection rates (*8*). Because structure-based imaging methods seem limited in their ability to locate cancer in the prostate, it is worthwhile to explore imaging methods that have a molecular or biochemical basis.

Several lines of research suggest the choline metabolic pathway to be a promising imaging target for prostate cancer (*9–15*). The detection of primary and metastatic

prostate cancer using PET and radiolabeled analogs of choline was first demonstrated by Hara et al. using ^{11}C-choline and ^{18}F-fluoroethylcholine (*16,17*). Another ^{18}F-labeled compound, fluorocholine, has also shown potential as an imaging agent for prostate cancer, with in vitro phosphorylation rates comparable to those of natural choline (*18–22*). In comparison to the commonly used oncologic tracer ^{18}F-FDG, ^{18}F-fluorocholine has demonstrated higher avidity for both androgen-dependent and androgen-independent prostate cancer (*21*). Areas of increased ^{18}F-fluorocholine uptake within the prostate have also correlated well with areas of malignancy on prostate biopsy (*20*). On the basis of these preliminary results, PET with ^{18}F-labeled choline analogs offers potential clinical value for localizing and staging prostate cancer.

In studies of ^{18}F-fluorocholine PET, scanning usually commences after a relatively brief delay (2–10 min) after tracer injection. (*18–21*). The use of relatively short uptake intervals is supported by studies demonstrating rapid blood-pool clearance and tissue uptake of ^{18}F-fluorocholine, as well as rapid phosphorylation by the enzyme choline kinase (*18,19*). Immediate imaging may also avoid potential imaging artifacts caused by accumulated ^{18}F radioactivity in the urinary bladder. However, the optimal timing for prostate PET using ^{18}F-fluorocholine has not yet been systematically evaluated, and the metabolism and clearance of ^{18}F-fluorocholine in benign and malignant tissue is not yet fully understood. For example, the cause of transient uptake and clearance of ^{18}F-fluorocholine from benign lymph nodes, in contrast to more durable retention in malignant sites, is not known (*21*). Although the rapid distribution of ^{18}F-fluorocholine may permit PET to be performed almost immediately after injection, delayed imaging could potentially improve lesion contrast in some areas of the body. The aim of this study was to evaluate whether 1-h delayed ^{18}F-fluorocholine PET could increase contrast between benign and malignant areas in the prostate.

MATERIALS AND METHODS

Subjects

The institutional review board approved the study before it began. Informed consent was obtained from all subjects before they entered the study. Twenty-six sequential subjects underwent dual-phase PET with ^{18}F-fluorocholine at our institution between July 2004 and June 2005. Twenty-three subjects had a history of prostate cancer, and 15 of these subjects had not yet received treatment for prostate cancer before PET. Of the remainder, 2 had undergone previous external-beam radiation therapy but had biopsy-proven recurrence in the prostate, and 6 had no clinical or biochemical (i.e., increasing serum PSA levels) evidence of recurrent disease after treatments that included radical prostatectomy (subject 22), external-beam radiation therapy (subjects 18, 19, 20, 23), brachytherapy (subject 20), and androgen suppression (subjects 18, 22, 23). For subjects who had not yet been treated, PET was performed within 8 wk of diagnosis. With the exception of 1 subject with bone metastases (subject 17), no subject had clinical or radiographic evidence of extraprostatic disease at the time of PET. In addition, 3 subjects who did not have a history of prostate cancer underwent dual-phase PET with ^{18}F-fluorocholine. Two of these subjects had a history of primary brain tumor, and 1 did not have a history of cancer.

Synthesis of ^{18}F-Fluorocholine

The radioactive tracer ^{18}F-fluorocholine was synthesized by fluorination of ditosylmethane with ^{18}F, followed by alkylation of fluorotosylmethane with dimethyl ethanol amine. The synthesis was automated and performed at an on-site cyclotron laboratory using a chemical process control unit (CTI/Siemens) (*23*). The radiochemical purity was greater than 99%.

PET

PET was performed using an SHR-22000 whole-body PET instrument (Hamamatsu Photonics). Subjects were positioned supine in the PET scanner. Whole-body transmission scans were acquired using two ^{68}Ge rod sources over 5 fields of view (FOVs) starting at the pelvis and proceeding cephalad. Transmission scanning at each FOV lasted 3 min. A 3.3–4 MBq/kg dose of ^{18}F-fluorocholine was then administered intravenously. After a delay of approximately 7 min, 2-dimensional emission scans were acquired over the same FOVs for 7 min each. On each scan, the first FOV was centered at the level of the pubic symphysis to include the prostate. After the whole-body scanning, the subjects voided in the restroom and then were repositioned in the scanner with the FOV centered over the pelvis. A single-FOV postinjection transmission scan was then acquired over 3 min. Approximately 1 h after tracer injection, a single-FOV emission scan of the pelvis was acquired over 7 min. Both initial whole-body and delayed pelvic images were reconstructed using ordered-subsets expectation maximization. Segmented attenuation correction was applied using the measured transmission data. Reconstruction resulted in voxels measuring 4 by 4 by 3.6 mm. Images were viewed and analyzed on a computer workstation using PET image analysis software (Medasys Data Systems).

Analysis

PET images were evaluated by 2 independent readers for tracer uptake in the prostate region. Neither reader was aware of the histopathology results at the initial reading. On PET images, the prostate was identified as a discrete region of uptake inferior and slightly posterior to the urinary bladder (Fig. 1). Visualized prostate volumes were segmented according to a sextant biopsy template into an upper (basal) one third, middle one third, and lower (apical) one third on each side. Region-of-interest analysis identified the sextant with highest measured activity on the initial whole-body and delayed pelvic images. The maximum standardized uptake value (SUVmax) in that sextant on both initial and delayed images was recorded. SUVmax was defined as the maximum measured activity divided by the injected radioactivity normalized to body weight. A retention index (%) was calculated as $100 \times$ (SUVmax [at 1 h after injection] $-$ SUVmax [at 7 min after injection])/SUVmax [at 7 min after injection].

The pathology results corresponding to sextant or whole-prostate analysis were reviewed to determine malignant involvement in each sextant. The malignant sextant having the highest standardized uptake value on initial and delayed images was classified as the dominant malignant region. In 5 subjects who subsequently underwent radical prostatectomy, the prostate was histologically examined using the step-section technique. The

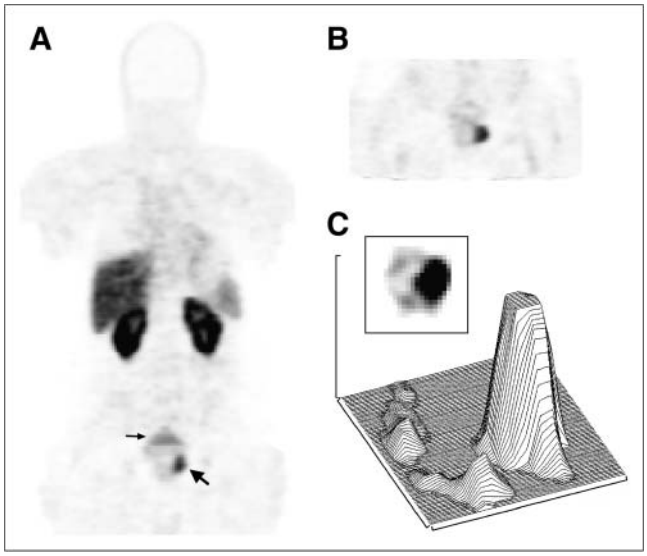

FIGURE 1. Subject 3, with histologically proven malignancy in left prostate lobe. (A) Coronal whole-body ^{18}F-fluorocholine PET image 7 min after injection shows focal uptake in left lobe of prostate (large arrow) corresponding to malignant lesion on biopsy. Increasing bladder activity is evident in second FOV of this image (small arrow). (B) Coronal image of pelvis 1 h after injection shows increasing activity in prostate lesion. Images are shown at same intensity. (C) Graph depicts distribution of SUVmax increase in transverse slice of prostate at midsection (inset: delayed transverse image). SUVmax in lesion increased by 22% (+4.4), whereas SUVmax in contralateral benign area decreased by 6% (−0.4).

formalin-fixed whole prostate was sectioned at regular 2.2-mm intervals. Thin slices from each section were mounted on large glass slides and stained with hematoxylin and eosin. Three alignment markers were placed on each slide to record the spatial orientation between slices. Areas of malignant tumor on each slide were manually segmented by a pathologist, and each slide was photographed to scale using a digital camera mounted on a stage. A model of each specimen showing the contour of the prostate surface and the location of tumors was created using surface-modeling software (3D-fit; i.Solutions, Inc.). A 3-dimensional model of the probable tumor volume based on PET images of the prostate was also rendered using software created for this purpose (SARGA; i.Solutions, Inc.) (Fig. 2). We compared these models to aid in correlating areas of uptake within the prostate on PET images to areas of malignancy in the specimen.

On PET images of the prostate, a probable benign region was defined either as a biopsy-negative sextant contralateral to the region of highest uptake or as the largest tumor-free region on whole-prostate step-section analysis. The SUVmax of the probable benign regions on the initial whole-body and delayed pelvic images was measured by region-of-interest analysis. It was not possible to define a probable benign region in 2 subjects because, at biopsy, malignancy was seen to involve all prostate sextants. The entire prostate was defined as a probable benign region in subjects who did not have a history of prostate cancer ($n = 3$) and subjects who had no evidence of disease after treatment for prostate cancer ($n = 6$). The SUVmax of each probable benign region and its corresponding location was recorded. In 15 subjects, both malignant and benign regions were identified within the prostate on the basis of histologic findings (i.e., a dominant malignant region and a probable benign region were present in the same prostate). A malignant-to-benign ratio for SUVmax was calculated for these subjects by dividing the SUVmax of the dominant malignant region by that of the probable benign region.

Differences in sample means were tested for significance using the Student t test. For paired measurements, differences in means were tested for significance using the paired t test. The linear relationship between 2 variables was assessed using the Pearson correlation coefficient. The ability of early and delayed uptake measurements to discriminate dominant malignant regions from probable benign regions was evaluated using receiver operating characteristic analysis. Statistical analysis was performed using JMP, version 5 (SAS Institute Inc.). All tests were 2-sided, and P values of less than 0.05 were considered significant.

RESULTS

Subject Characteristics

The characteristics of each subject are listed in Table 1. The average age of subjects with newly diagnosed or

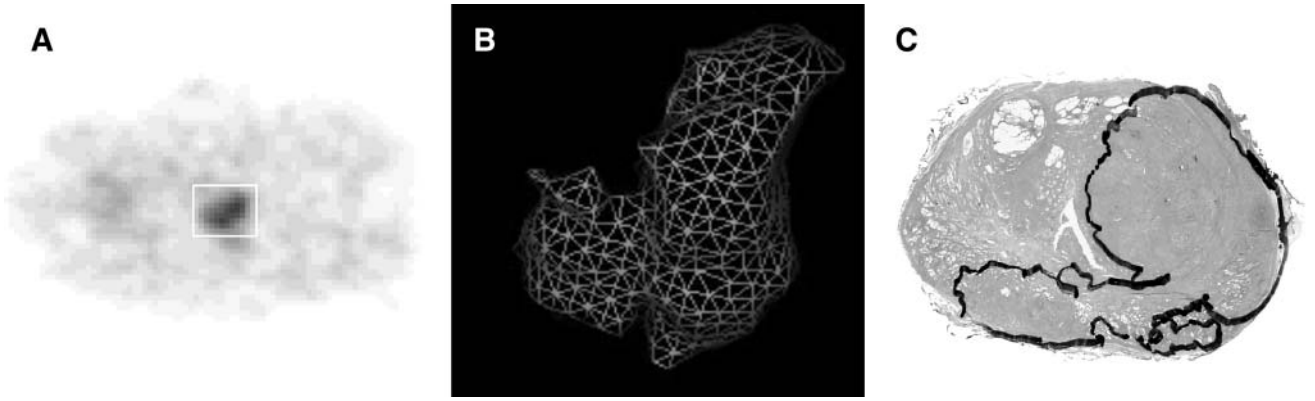

FIGURE 2. Histopathologic correlation of ^{18}F-fluorocholine PET of prostate. (A) One-hour delayed PET scan of pelvis of subject 14 shows increased ^{18}F-fluorocholine uptake in prostate (enclosed by white box). (B) Computer-rendered surface model based on PET images depicts 3-dimensional configuration of highest activity within prostate. (C) Low-power micrograph of prostate specimen shows left-sided tumor with contralateral tumor extension (outlined in black), morphologically resembling corresponding PET and computer-rendered images.

TABLE 1
Subject Characteristics

Patient no.	Age (y)	Serum PSA (ng/dL)	DMR SUVmax at T1	DMR SUVmax at T2	PBR SUVmax at T1	PBR SUVmax at T2	DMR retention index (%)	PBR retention index (%)	T2–T1 interval (min)	Gleason score	Prior treatment
1	66	6	5.4	6.41	7.82	6.98	19	−11	45	3 + 4	None
2	67	10	6.51	6.51	5.01	4.74	0	−5	61	3 + 3	None
3	70	29	19.66	24.04	5.68	5.33	22	−6	50	5 + 4	None
4	59	25	6.69	11.12	9.63	6.75	66	−30	47	3 + 4	XRT
5	77	4	4.64	5.08	2.5	3.12	9	25	16	5 + 5	None
6	71	6	6.09	6.34	5.15	4.88	4	−5	44	3 + 3	None
7	63	7	9.25	10.55	5.6	3.7	14	−34	45	3 + 4	None
8	78	13	6.19	6.68	4.32	4.55	8	5	43	3 + 4	None
9	83	22	4.74	5.75	5.5	4.8	21	−13	40	4 + 3	None
10	60	22	3.3	3.88	2.81	2.22	18	−21	43	4 + 5	None
11	65	5	5.44	5.79	4.63	3.74	6	−19	45	3 + 4	None
12	67	1.2	6.19	6.68	4.32	4.86	8	13	47	3 + 4	XRT
13	68	7	5.74	6.36	4.19	3.9	11	−7	50	3 + 4	None
14	64	12	6.9	7.32	5.35	4.77	6	−11	45	5 + 4	None
15	67	29	9.12	9.15	6.09	4.22	0	−31	44	3 + 3	None
16	66	5	14.53	16.44			13		53	4 + 5	None
17	47	272	8.51	9.41			11		42	4 + 5	None
18	60	0			4.9	3.54		−28	45	3 + 3	XRT, HT
19	70	0			2.39	2.03		−15	45	3 + 4	XRT
20	72	0			4.74	2.94		−38	52	3 + 3	XRT
21	73	0			3.57	2.52		−29	47	3 + 3	HT, brachy
22	77	0			2.52	1.39		−45	47	3 + 4	RP
23	72	0			2.32	1.63		−30	45	3 + 4	XRT, HT
24	52				4.19	3.32		−21	21		None
25	67				5.6	4.89		−13	50		None
26	38				5.38	3.92		−27	75		None

DMR = dominant malignant region; PBR = probable benign region; T1 = time of initial PET image; T2 = time of delayed PET image; XRT = external-beam radiation therapy; HT = hormonal therapy; RP = radical prostatectomy; brachy = brachytherapy.

recurrent prostate cancer was 67 y (range, 38–83 y). The average age of subjects who had no evident disease after treatment was 71 y (range, 60–77 y). The median serum PSA in subjects with newly diagnosed or recurrent prostate cancer was 10 ng/dL (range, 1.2–272 ng/dL). The median Gleason sum was 7 (range, 6–10). No significant correlations were observed between SUVmax, age, serum PSA, and Gleason sum.

PET Images

The average interval from injection to initial whole-body PET was 7 min. The average interval from injection to delayed pelvic imaging was 57 min. Six subjects (subjects 18−23; Table 1) had been previously treated for prostate cancer but had no clinical or biochemical evidence of recurrent disease at the time of PET. In these subjects, uptake in the prostate was relatively low and decreased over time. Mean SUVmax in the prostate on the initial and delayed PET images was 3.4 and 2.3, respectively, in these subjects. Three subjects (subjects 24−26) did not have a history of prostate cancer. Highest uptake in the prostate on initial and delayed PET images occurred in the same sextant in each of these subjects. Uptake within these regions decreased over time, with a mean SUVmax of 5.0 and 4.0 on initial and delayed images, respectively.

The remaining 17 subjects (subject 1−17) currently had prostate cancer but had not yet received treatment ($n = 15$) or had recurrent cancer after local external-beam radiation therapy ($n = 2$). In 1 subject with a serum PSA level of 272 ng/dL (subject 17), bone scintigraphic evidence of skeletal metastases corresponded to areas of increased skeletal uptake on the initial whole-body ^{18}F-fluorocholine PET images. The remaining subjects did not show extraprostatic sites of increased ^{18}F-fluorocholine uptake suggestive of metastases.

Visual interpretation of the initial and delayed PET images was not problematic. The 2 independent readers had experience with interpreting ^{18}F-fluorocholine PET images (*20,24*). Identification of the prostate gland and the prostate sextant with highest uptake was facilitated by the consistent position of the prostate in the pelvis and the higher uptake in the prostate than in surrounding pelvic structures at the same level. For each subject, the readers agreed on the prostate sextant demonstrating highest uptake, and concordance in measured SUVmax was found by region-of-interest analysis.

A total of 17 dominant malignant regions and 24 probable benign regions were identified. The mean SUVmax for dominant malignant regions increased significantly between the initial and delayed ^{18}F-fluorocholine PET scans, from 7.6 to 8.6 (mean retention index, +14%; 95% confidence interval, 6%–22%, $P = 0.002$) (Fig. 3A). The mean SUVmax for probable benign regions decreased significantly between the initial and delayed ^{18}F-fluorocholine PET scans, from 4.8 to 3.9 (mean retention index, −17%; 95% confidence interval, −10% to −23%; $P < 0.001$) (Fig. 3B). SUVmax differed significantly between the dominant malignant and probable benign regions on the initial scan (mean difference, 2.8; 95% confidence interval, 1.0–4.7; $P = 0.01$) and on the delayed scan (mean difference, 4.7; 95% confidence interval, 2.6–6.9; $P = 0.001$).

In subjects for whom histologic analysis found both benign and malignant regions in the prostate (subjects 1–15), the mean malignant-to-benign ratio increased from 1.4 on the initial images to 1.8 on the delayed images (Table 2). This increase was statistically significant ($P = 0.003$). In these subjects, the difference in mean SUVmax between dominant malignant regions and probable benign regions was statistically significant on delayed imaging ($P = 0.009$) but not on initial imaging ($P = 0.09$). Mean retention index also differed significantly between dominant malignant regions and probable benign regions in a paired analysis limited to these 15 subjects (+14% vs. −10%, respectively, $P = 0.003$).

The area under the receiver operating characteristic curve for distinguishing dominant malignant regions from probable benign regions based on measured SUVmax on initial whole-body images was 0.81. The area under the curve for distinguishing dominant malignant regions from probable benign regions based on measured SUVmax on delayed pelvic images was 0.92. The area under the curve for distinguishing dominant malignant regions from probable benign regions based on the retention index was 0.93 (Fig. 4).

TABLE 2
Malignant-to-Benign Ratio of SUVmax at T1 and T2 in 15 Subjects

Patient no.	Malignant-to-benign ratio	
	T1	T2
1	0.69	0.92
2	1.30	1.37
3	3.46	4.51
4	0.69	1.65
5	1.85	1.63
6	1.18	1.30
7	1.65	2.85
8	1.43	1.47
9	0.86	1.20
10	1.17	1.75
11	1.17	1.55
12	1.43	1.37
13	1.37	1.63
14	1.29	1.53
15	1.50	2.17

T1 = time of initial PET image; T2 = time of delayed PET image.

DISCUSSION

In vitro and in vivo studies have provided substantial evidence that increased choline metabolism is a prominent feature of prostate cancer (*9–14*). Prostate cancer cells appear to contain higher levels of choline metabolites (e.g., phosphocholine and phosphatidylcholine) than do normal prostate epithelial and stromal cells (*11*). In vivo studies using 3-dimensional MRI spectroscopy have shown choline metabolite levels to be almost twice as high in areas of cancer as in areas of benign prostatic hyperplasia and normal tissue (*13*). Increased levels of choline metabolites in malignant cells are attributable to alterations in the activity of the choline kinase enzyme. Choline kinase catalyzes the phosphorylation of choline to produce phosphocholine. In eukaryotic cells, this enzyme pathway

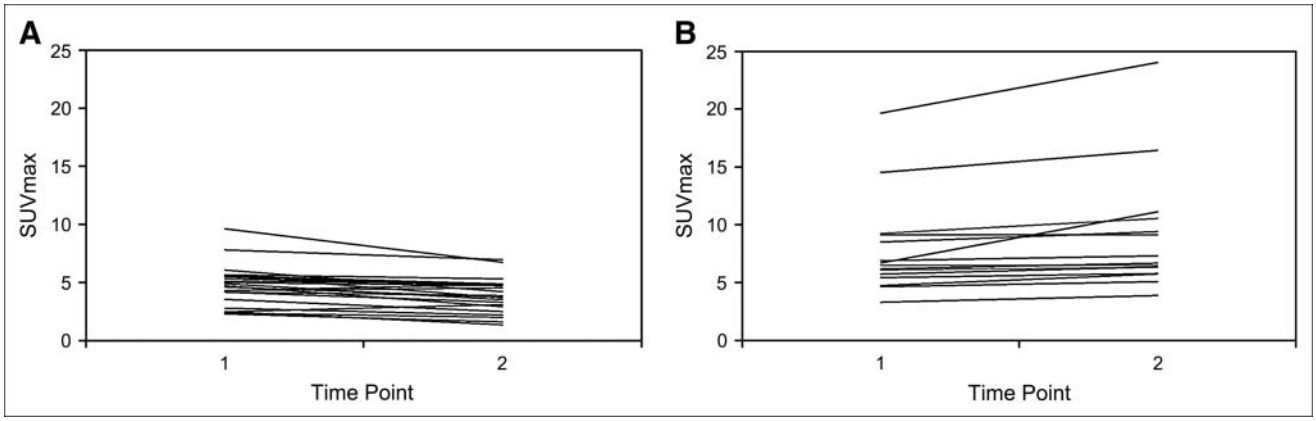

FIGURE 3. Plots of SUVmax in probable benign regions (A) and dominant malignant regions (B) on initial (time point 1) and delayed (time point 2) ^{18}F-fluorocholine PET images of prostate.

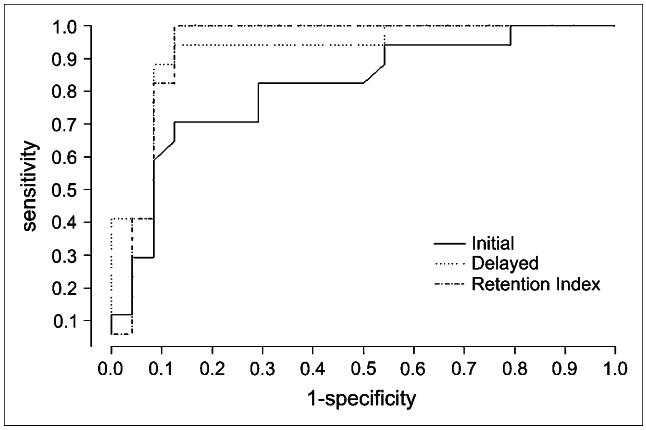

FIGURE 4. Relative accuracy of different SUVmax measurements. Receiver operating characteristic curve for distinguishing dominant malignant region from probable benign region is based on SUVmax measurements on initial and delayed PET scans and their percentage difference (i.e., retention index).

serves as the primary source of phosphatidylcholine and other important cell membrane constituents. Human tumor–derived cell lines of breast, colon, lung, and prostate cancer have higher choline kinase activity than do appropriate nontumor cells (*14,15*). As an avid substrate for choline kinase, ^{18}F-fluorocholine also undergoes phosphorylation to produce ^{18}F-phosphorylfluorocholine (*18*). In cultured PC-3 (human prostate cancer) cells incubated with ^{18}F-fluorocholine, most of the intracellular ^{18}F radioactivity is accounted for by the production of ^{18}F-phosphorylfluorocholine (*18*). The accumulation of ^{18}F-fluorocholine over time in malignant lesions, as observed in this study, is explainable by the metabolic trapping of ^{18}F-fluorocholine due to phosphorylation.

Although this mechanism explains the increase in ^{18}F-fluorocholine uptake in dominant malignant regions, it does not necessarily explain the decrease in ^{18}F-fluorocholine uptake over time in probable benign regions. In the current study, the decrease in ^{18}F-fluorocholine uptake in probable benign regions was comparable in magnitude to the increase in uptake in dominant malignant regions. One potential explanation is the dephosphorylation of ^{18}F-phosphorylfluorocholine by prostatic acid phosphatase, an enzyme specific to prostate tissues. Normal prostate tissue and tissue affected by benign prostatic hyperplasia contain higher levels of prostatic acid phosphatase than does malignant prostate tissue (*25*). Phosphocholine is known to be an avid substrate for prostatic acid phosphatase even though it is relatively resistant to other phosphatases (*26*). Because ^{18}F-phosphorylfluorocholine is structurally similar to phosphocholine, it may have the potential to serve as a substrate for prostatic acid phosphatase as well. This catabolic pathway could therefore explain the decrease in ^{18}F-fluorocholine uptake over time in areas of the prostate containing benign tissue. The fact that prostatic acid phosphatase activity is reduced in transformed prostate cells is also consistent with increases in ^{18}F-fluorocholine uptake observed in areas of malignancy. Further research is necessary to determine the actual mechanisms responsible for these observations.

The larger areas under the receiver operating characteristic curve for delayed and dual-phase imaging suggest that imaging at these times may be superior to early imaging for distinguishing benign from malignant areas in the prostate. Although in many cases the sextant demonstrating the highest uptake on either the initial or delayed PET scan corresponded to an area of malignancy, our study had 3 subjects (subjects 1, 4, and 12) in whom the region of highest prostatic activity on early imaging corresponded to a histopathologically benign area. In each of these subjects, SUVmax in the corresponding sextant decreased over the 2 time points (i.e., retention index $< 0\%$), indicating that these regions were indeed benign. In contrast, malignant areas consistently demonstrated stable or increasing uptake over time. In subjects in whom it was possible to identify both a benign and a malignant region within the prostate, the difference between the SUVmax of the dominant malignant region and that of the probable benign region was statistically significant on delayed imaging but not on initial imaging. On the basis of these results, optimal scanning of the prostate with ^{18}F-fluorocholine PET may involve imaging at dual times or after a delay to improve the contrast between malignant and benign (and possibly hyperplastic) tissues.

One potential drawback to delayed imaging with ^{18}F-fluorocholine is the accumulation of radioactivity in the bladder and the consequent potential for obscuring of the prostate gland. In contrast to ^{11}C-labeled choline, ^{18}F-fluorocholine undergoes relatively consistent excretion by the renal system, possibly leading to the accumulation of significant bladder radioactivity over time. Fortunately, accumulated radioactivity in the bladder can be minimized by several methods, such as timed voiding or hydration (to dilute the radioactivity), as well as the insertion of a urinary bladder catheter as has been used for ^{18}F-FDG PET of the pelvis (*27*). In the current study, subjects had been asked to void before delayed imaging, and the presence of bladder radioactivity did not impair interpretation.

The intraprostatic localization of cancer has been attempted with other metabolic imaging techniques. For example, MRI spectroscopy has been used to characterize prostate lesions on the basis of choline and citrate content (*5,13,28*). For this procedure, an endorectal probe is typically required to obtain spectroscopic information of sufficient quality. Although the spatial resolution of this technique is similar to PET, only a small volume can be imaged at one time, making this technique impractical for oncologic staging. Further research is necessary to determine the relative accuracies of both imaging modalities and whether the information obtained by these modalities is complementary.

Several points should be considered when interpreting the study results. First, the evaluation of ^{18}F-fluorocholine PET was limited to prostate imaging at 2 times. The optimal timing of ^{18}F-fluorocholine PET for oncologic staging (to detect nodal and distant metastatic disease) was not addressed by this study. Furthermore, to maintain the tolerability of this procedure, 1-h dynamic imaging of the prostate was not performed. Presumably, similar results could be achieved using dynamic PET, although this remains to be tested. Second, there may be a question as to why an increase in the SUVmax of probable benign regions was observed in 3 of the subjects (subjects 5, 8, and 12). Although the SUVmax of these probable benign regions was relatively lower than the average SUVmax of dominant malignant regions, an interval increase in uptake in probable benign regions raises the possibility that some benign tissues can accumulate ^{18}F-fluorocholine over time. However, because the pathology data for these 3 subjects were obtained from biopsy, it is also possible that sampling error could have resulted in a malignant sextant's being misclassified as a probable benign region. Unfortunately, whole-prostate histologic examination was not performed for these subjects, and therefore it is not possible to confirm this possibility. Finally, the current study used ^{18}F-fluorocholine exclusively for prostate PET. It is conceivable that similar patterns of uptake can be observed using other choline analogs such as ^{18}F-fluoroethylcholine and ^{11}C-choline. Delayed PET of the prostate with these choline analogs deserves further study. However, with regard to ^{11}C-choline, the short half-life of ^{11}C (20 min) may limit its utility in delayed PET.

In this study, all prostate sextants with malignant involvement demonstrated stable or increasing ^{18}F-fluorocholine uptake over time. On the basis of these results, dual-phase ^{18}F-fluorocholine PET appears advantageous for identifying the most likely region of malignancy within the prostate. However, further study is needed to determine the overall accuracy of ^{18}F-fluorocholine PET for mapping the extent of malignancy in the prostate. A larger study directly comparing ^{18}F-fluorocholine PET findings with whole-prostate histopathologic findings is needed to evaluate ^{18}F-fluorocholine PET as a technique for tumor mapping. Nevertheless, knowing the location of a single "dominant" malignant lesion in the prostate may still have clinical value. For example, knowing the most likely location of malignancy in the prostate may allow prostate biopsies to be directed toward those regions, thus potentially increasing the diagnostic accuracy of biopsy. For radiation therapy, it may be possible to target a region identified by ^{18}F-fluorocholine PET to receive a higher radiation dose and thus increase the likelihood of tumor eradication. The advent of advanced conformal techniques for the planning and delivery of external-beam radiation therapy has made it possible to enhance the dose of radiation to specific lesions within the prostate while maintaining a safer therapeutic dose to the remainder of the gland (*1,2*). Further study of the appropriate subject populations (e.g., subjects with elevated levels of serum PSA) is necessary to determine the potential role of ^{18}F-fluorocholine PET in these settings.

CONCLUSION

On dual-phase PET of the prostate, areas of malignancy demonstrated stable or increasing ^{18}F-fluorocholine uptake over time, whereas most areas containing benign tissue demonstrated a corresponding decrease. Compared with ^{18}F-fluorocholine PET at earlier times, 1-h delayed PET may improve differentiation between benign and malignant areas of the prostate. Decreases in ^{18}F-fluorocholine uptake in areas that contain benign prostate tissue may be the result of higher phosphatase activity in these areas than in areas of malignant involvement.

ACKNOWLEDGMENTS

This study was supported by NIH/NCI grant R41CA110121 and NIH grant RR-16467. The findings and conclusions expressed in this article do not necessarily represent the views of The Queen's Medical Center.

REFERENCES

1. Pickett B, Vigneault E, Kurhanewicz J, et al. Static field intensity modulation to treat a dominant intra-prostatic lesion to 90 Gy compared to seven field 3-dimensional radiotherapy. *Int J Radiat Oncol Biol Phys.* 1999;44:921–929.
2. Pouliot J, Kim Y, Lessard E, et al. Inverse planning for HDR prostate brachytherapy used to boost dominant intraprostatic lesions defined by magnetic resonance spectroscopy imaging. *Int J Radiat Oncol Biol Phys.* 2004;59:1196–1207.
3. Zelefsky MJ, Fuks Z, Hunt M, et al. High dose radiation delivered by intensity modulated conformal radiotherapy improves the outcome of localized prostate cancer. *J Urol.* 2001;166:876–881.
4. el-Gabry EA, Halpern EJ, Strup SE, et al. Imaging prostate cancer: current and future applications. *Oncology (Williston Park).* 2001;15:325–336.
5. Wefer AE, Hricak H, Vigneron DB, et al. Sextant localization of prostate cancer: comparison of sextant biopsy, magnetic resonance imaging and magnetic resonance spectroscopic imaging with step section histology. *J Urol.* 2000;164:400–404.
6. Basillote JB, Armenakas NA, Hochberg DA, et al. Influence of prostate volume in the detection of prostate cancer. *Urology.* 2003;61:167–171.
7. Rabbani F, Stroumbakis N, Kava BR, et al. Incidence and clinical significance of false-negative sextant prostate biopsies. *J Urol.* 1998;159:1247–1250.
8. Naughton CK, Miller DC, Mager DE, et al. A prospective randomized trial comparing 6 versus 12 prostate biopsy cores: impact on cancer detection. *J Urol.* 2000;164:388–392.
9. Heerschap A, Jager GJ, van der Graaf M, et al. In vivo proton MR spectroscopy reveals altered metabolite content in malignant prostate tissue. *Anticancer Res.* 1997;17:1455–1460.
10. Ackerstaff E, Pflug BR, Nelson JB, et al. Detection of increased choline compounds with proton nuclear magnetic resonance spectroscopy subsequent to malignant transformation of human prostatic epithelial cells. *Cancer Res.* 2001;61:3599–3603.
11. Cornel EB, Smits GA, Oosterhof GO, et al. Characterization of human prostate cancer, benign prostatic hyperplasia and normal prostate by in vitro ^{1}H and ^{31}P magnetic resonance spectroscopy. *J Urol.* 1993;150:2019–2024.
12. Fowler AH, Pappas AA, Holder JC, et al. Differentiation of human prostate cancer from benign hypertrophy by in vitro ^{1}H NMR. *Magn Reson Med.* 1992;25:140–147.
13. Kurhanewicz J, Vigneron DB, Hricak H, et al. Three-dimensional H-1 MR spectroscopic imaging of the in situ human prostate with high (0.24-0.7-cm^{3}) spatial resolution. *Radiology.* 1996;198:795–805.
14. Ramirez de Molina A, Rodriguez-Gonzalez A, Gutierrez R, et al. Overexpression of choline kinase is a frequent feature in human tumor-derived cell

lines and in lung, prostate, and colorectal human cancers. *Biochem Biophys Res Commun.* 2002;296:580–583.
15. Aboagye EO, Bhujwalla ZM. Malignant transformation alters membrane choline phospholipid metabolism of human mammary epithelial cells. *Cancer Res.* 1999; 59:80–84.
16. Hara T, Kosaka N, Kishi H. PET imaging of prostate cancer using carbon-11-choline. *J Nucl Med.* 1998;39:990–995.
17. Hara T, Kosaka N, Kishi H. Development of (18)F-fluoroethylcholine for cancer imaging with PET: synthesis, biochemistry, and prostate cancer imaging. *J Nucl Med.* 2002;43:187–199.
18. DeGrado TR, et al. Synthesis and evaluation of (18)F-labeled choline analogs as oncologic PET tracers. *J Nucl Med.* 2001;42:1805–1814.
19. DeGrado TR, Reiman RE, Price DT, et al. Pharmacokinetics and radiation dosimetry of ^{18}F-fluorocholine. *J Nucl Med.* 2002;43:92–96.
20. Kwee SA, Coel MN, Lim J, et al. Prostate cancer localization with 18fluorine fluorocholine positron emission tomography. *J Urol.* 2005;173:252–255.
21. Price DT, Coleman RE, Liao RP, et al. Comparison of [^{18}F]fluorocholine and [^{18}F]fluorodeoxyglucose for positron emission tomography of androgen dependent and androgen independent prostate cancer. *J Urol.* 2002;168: 273–280.
22. Schmid DT, John H, Zweifel R, et al. Fluorocholine PET/CT in subjects with prostate cancer: initial experience. *Radiology.* 2005;235:623–628.
23. Lim J, Dorman E, Cabral C. Automated production of [^{18}F]FECh and [^{18}F]FCH: preparation and use of [^{18}F]fluoroalkane sulfonates and fluoroalkylation agents [abstract]. *J Labelled Compds Radiopharm.* 2003;46:S403.
24. Kwee SA, Coel MN, Lim J, et al. Combined use of F-18 fluorocholine positron emission tomography and magnetic resonance spectroscopy for brain tumor evaluation. *J Neuroimaging.* 2004;14:285–289.
25. Hakalahti L, Vihko P, Henttu P, et al. Evaluation of PAP and PSA gene expression in prostatic hyperplasia and prostatic carcinoma using northern-blot analyses, in situ hybridization and immunohistochemical stainings with monoclonal and bispecific antibodies. *Int J Cancer.* 1993;55:590–597.
26. Serrano JA, Wasserkrug HL, Serrano AA, et al. The histochemical demonstration of human prostatic acid phosphatase with phosphorylcholine. *Invest Urol.* 1977;15:123–136.
27. Leisure GP, Vesselle HJ, Faulhaber PF, et al. Technical improvements in fluorine-18-FDG PET imaging of the abdomen and pelvis. *J Nucl Med Technol.* 1997; 25:115–119.
28. Kurhanewicz J, Swanson MG, Nelson SJ, et al. Combined magnetic resonance imaging and spectroscopic imaging approach to molecular imaging of prostate cancer. *J Magn Reson Imaging.* 2002;16:451–463.